

# RESTORATION OF MICROSTRUCTURE AND MECHANICAL PROPERTIES OF LEAD-FREE BISMUTH CONTAINING SOLDER JOINTS AFTER ACCELERATED RELIABILITY TESTING USING A THERMAL TREATMENT

André M. Delhaise<sup>1,2,a</sup>, Mikaella Brillantes<sup>2</sup>, Ivan Tan<sup>1</sup>, Polina Snugovsky<sup>1</sup>, Jeff Kennedy<sup>1</sup>, David Hillman<sup>3</sup>, Stephan Meschter<sup>4</sup>, David Adams<sup>3</sup>, Milea Kammer<sup>5</sup>, Ivan Straznický<sup>6</sup>, Doug D. Perovic<sup>2</sup>

<sup>1</sup>Celestica, <sup>2</sup>Department of Materials Science & Engineering, University of Toronto, <sup>3</sup>Rockwell-Collins, <sup>4</sup>BAE Systems, <sup>5</sup>Honeywell Aerospace, <sup>6</sup>Curtiss-Wright  
adelhais@celestica.com

## ABSTRACT

Bismuth (Bi)-containing solder alloys have emerged as prime candidates to replace traditional lead (Pb)-free alloys such as SAC 305 (Sn-3.0Ag-0.5Cu). These alloys show stability in mechanical properties after aging, whereas the strength of SAC degrades over time. This finding prompted the development of a patented process in which the Bi-bearing alloy is subjected to a short above-solvus thermal treatment, to extend the life of the solder joint and improve device reliability. During this thermal treatment, all Bi in the alloy dissolves and diffuses through the  $\beta$ -Sn matrix to produce a homogenous microstructure with uniformly sized and distributed Bi precipitates, as well as an equiaxed  $\beta$ -Sn grain structure. In our most recent study, after accelerated thermal cycling (ATC) between  $-40^{\circ}\text{C}$  and  $70^{\circ}\text{C}$ , preconditioned Violet (Sn-2.25Ag-0.5Cu-6.0Bi) solder joints demonstrated a 15% improvement in characteristic life over their as-assembled counterparts; this was not the case for SAC 305.

In addition to preconditioning, it is proposed that the thermal treatment may 'restore' the microstructure and properties of the alloy after some time in service. Three assembly conditions, each representing some point in the product's life cycle, were analyzed either as-is, or after a restoration treatment. These conditions were as-assembled (early life), room temperature aged (long-term storage), and reliability tested (emulating long-term usage). Room temperature aging was conducted for approximately one year, and reliability testing consisted of alternating ATC (~100 cycles) and vibration (~100,000 cycles); testing was terminated after 2000 ATC cycles and 2 million vibration cycles. Ball Grid Array (BGA) and Plastic Leaded Chip Carrier (PLCC) components were analyzed; alloys under test were SAC 305 and Violet. Scanning Electron Microscopy (SEM) and Electron Backscatter Diffraction (EBSD) were utilized to study changes to alloy microstructure. The mechanical behavior of the joints (hardness) was analyzed using nanoindentation.

Key words: heat treatment, restoration, bismuth, nanoindentation

## INTRODUCTION

With the introduction of legislation such as the Restriction of Hazardous Substances (RoHS), lead free (Pb-free) solder alloys containing tin (Sn), silver (Ag), and copper (Cu), also

referred to as SAC, have emerged as the primary interconnection materials in electronic devices. However, these alloys are unsuitable for many applications and certain high-reliability industries, such as the aerospace, defence, and automotive sectors, have been granted temporary exemptions from transitioning to Pb-free per RoHS requirements. Several detrimental features of SAC alloys are as follows:

- **Higher melting point** – Sn-3.0Ag-0.5Cu (SAC 305) melts at  $217^{\circ}\text{C}$ , which is roughly  $34^{\circ}\text{C}$  higher than eutectic Sn-Pb (Sn-37Pb). This results in higher processing temperatures in manufacturing (typically  $240$ - $245^{\circ}\text{C}$ ), which may cause thermal damage to the printed circuit board (PCB) and components. In addition, new failure modes such as pad cratering<sup>1</sup> become prevalent as higher  $T_g$  boards become necessary for assembly.
- **Increased cost** – SAC 305 contains a small amount (3%) of Ag, which increases the cost of the alloy. In addition, the increase in melting point increases the energy expenditure required for assembly processes.
- **Reduced reliability** – Pb-free alloys contain intermetallic compounds (IMCs) such as  $\text{Ag}_3\text{Sn}$ . These are brittle phases that diminish the toughness of the alloy and can reduce solder joint reliability in some product use environments.
- **Degradation of properties over time** – Pb-free alloys experience coarsening of microstructure when aged<sup>2,3,4,5,6</sup>, which lowers the strength and creep resistance over time, and subsequently reduces reliability long-term reliability.

Additional alloying elements such as bismuth (Bi), antimony (Sb) and indium (In) have been considered for inclusion in the alloy to produce a more dependable, robust, and reliable solder alloy. Bi is particularly attractive as it decreases the melting point<sup>2,3,7</sup> of the solder, which reduces the energy consumption during assembly, allows for standard  $T_g$  boards to be used, and reduces damage to temperature-sensitive components. In addition, the strength of Bi-bearing alloys is maintained over time<sup>2,3,8,9</sup> and generally the reliability is improved over SAC.

In our earlier work<sup>10,11</sup>, we presented results from a process in which the Bi-containing alloy solder joint, after assembly,

is subjected to a short-term thermal treatment. The as-solidified microstructure is dendritic and non-uniform, with Bi precipitation localized to the interdendritic spaces (**Figure 1a**). The thermal treatment allows for all Bi precipitates to be dissolved in the Sn matrix and, upon cooling, reprecipitate into a more robust, uniform microstructure<sup>10</sup> (**Figure 1b**).

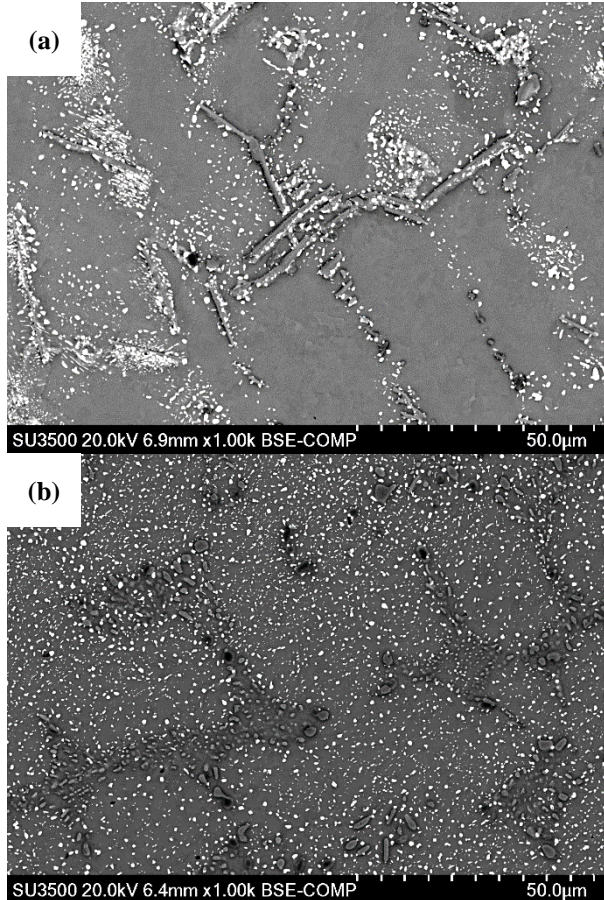


**Figure 1:** Microstructure evolution of Violet (Sn-2.25Ag-0.5Cu-6.0Bi) after aging<sup>10</sup>. As-cast (a); aged at 120°C for 300 hours, showing increased uniformity of Bi precipitation (b).

It was found that the alloy under test, Violet (Sn-2.25Ag-0.5Cu-6.0Bi) underwent extensive recrystallization (**Figure 2a&b**) and demonstrated a marked increase in creep resistance (**Figure 2c**) after the thermal treatment<sup>10</sup>. In addition, the Weibull characteristic life of the alloy improved by roughly 15%<sup>11</sup> after the thermal treatment after ATC between -40°C and +70°C (**Figure 2d**). These findings demonstrated the potential of this process to be used to extend the life of the alloy in the field. It has also been postulated that this treatment may be used periodically during the service life as an ‘alternative to repair’ process – it has been shown that during extended aging times simulating product usage conditions (70°C) that Bi precipitates may undergo coarsening via Ostwald ripening, which may degrade reliability (**Figure 3a**) – Bi is harder than the Sn matrix and larger particles may embrittle the

alloy<sup>10</sup>. Ostwald ripening may also occur after extended room temperature storage<sup>2</sup> (**Figure 3b**), and damage may accumulate as a result of environmental stresses such as temperature cycling and vibration, weakening the microstructure.

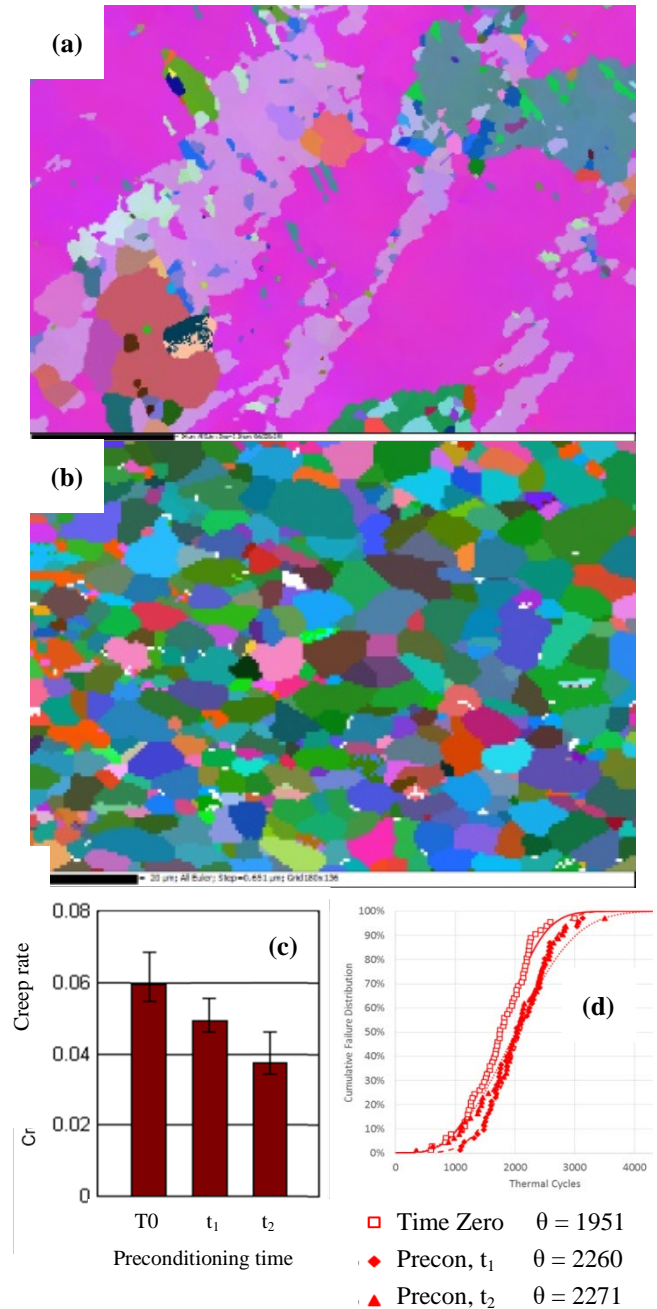


**Figure 2:** Effects of preconditioning on the microstructure, properties and reliability of Violet. Electron Backscatter Diffraction (EBSD) maps<sup>10</sup> showing the coarse as-solidified grain structure (a) recrystallizes after aging above solvus (b). The creep resistance increases<sup>10</sup> after aging (c), as does the characteristic life<sup>11</sup> after ATC (d).

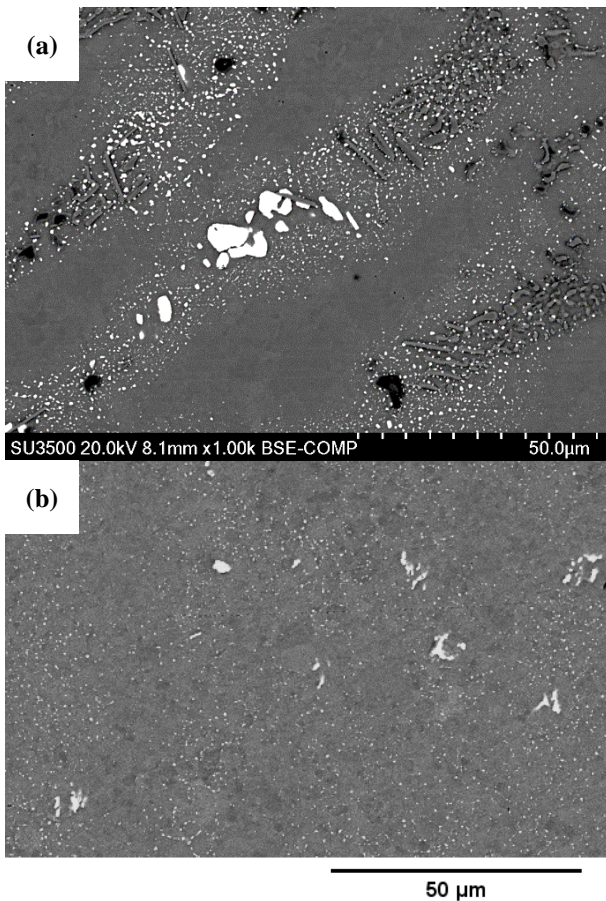


**Figure 3:** Evidence of Ostwald ripening of Bi-containing alloys after aging. Violet, after aging at 70°C for 300 hours<sup>10</sup> (a); Sn-5Bi, after aging at room temperature for 168 days<sup>2</sup> (b).

In addition, there is interest in the development of combined environment test protocols, such as combined accelerated thermal cycling (ATC) and vibration. This better emulates real-life conditions compared with performing each test separately, however numerous challenges exist. Combined test protocol results will be affected by recrystallization of lead-free solder joints confounding ATC results let alone adding vibration<sup>12</sup>. In addition, the time scales of each test vary significantly, with ATC typically requiring months to complete, compared with days or weeks for vibration; this makes sequential tests conceptually more viable. Variance in sequencing is of consequence and may affect performance in combined environments<sup>13</sup>.

The authors have established a three-phase approach intended to generate relationships between the multiple sources of variation in the design variables (such as test temperature) as a roadmap towards a combined environment test plan. The sample sizes, alloy composition, and surface finish combinations at the various temperatures or temperature ranges under study are shown in **Table 1**. The results from Test Phases 1a and 1b were previously presented<sup>14,15</sup>.

**Table 1:** Overall Project Test Plan

Planned Test Phase	Test Temp.	SAC 305		SnPb	Violet
		ENIG	OSP	ENIG	ENIG
1a Sweep & Overstress	-55°C	1	1	0	0
	25°C	2	1	0	0
	75°C	1	1	0	0
	125°C	1	1	0	0
1b Accelerated Life Test	25°C	3	0	2	1
	75°C	2	0	2	2
	125°C	2	0	1	1
2 Combined Test (Pilot Run)	-55°C to 125°C + Vibe (75°C)	1	0	1	1
2 Combined Test (Full Run)	-55°C to 125°C (ATC only)	2	0	2	2
	-55°C to 125°C + Vibe (75°C)	4	0	4	4
	-40°C to 85°C (ATC only)	4	0	4	4
	-40°C to 85°C (ATC only) + Precon.	4	0	0	4
	-40°C to 85°C + Vibe (75°C)	4	0	4	4
	-40°C to 85°C + Vibe (75°C) + Precon.	4	0	0	4

Phase 1a focused on isothermal sweep and overstress at the boundary temperatures and at important intermediate temperatures to understand the range of failure times, the relative energy required to generate failures and to confirm consistent failure modes at all temperatures<sup>14</sup>. Phase 1b consisted of isothermal and constant strain range harmonic testing at approximately 0.9-1.0G input and 300 µε target strain, with two objectives: to develop a relationship between microstrain and cycles to failure at the various test temperatures from Phase 1a, except -55°C, and determine the appropriate constant strain range and temperature protocol to be used for Phase 2<sup>15</sup>.

Phase 2 is intended to consist of sequential thermal cycling and constant strain range harmonic testing injected at 75°C once per week for a target duration of 100,000 cycles per week (initially using the same parameters as Phase 1b) over two separate temperature ranges (-40°C to 85°C as well as -55°C to 125°C). For the former temperature range, preconditioning will be performed on select units. It was previously shown<sup>11</sup> that the harsher cycle range (-55°C to 125°C) has no effect on reliability, likely because the cycle itself has the same effect on the microstructure as preconditioning. Phase 2 will enable the study of both the metallurgical changes over the ATC cycles, combined effects of ATC and vibration, and preconditioning with relation to that metallurgy and failure mode.

A preliminary pilot run, which tested this combined sequential methodology has been completed and is the focus of this paper. Results from this test will serve as a benchmark for the main Phase 2 run. This combined test, better simulating practical product life than an isothermal

aging test or singular (ATC or vibrate separately) reliability tests, is an ideal opportunity to test the efficacy of the aforementioned thermal treatment as a tool for restoration of solder joints after some time in service.

**TEST OBJECTIVE**

Our previous work indicated that a heat treatment may be used immediately after assembly to homogenize the microstructure of Bi-bearing solder alloys and, in certain cases, improve reliability. It has also been established that during the product life cycle, the microstructure of these alloys may become degraded via Ostwald ripening of the Bi precipitates, which may have a deleterious effect on reliability. To that end, it is proposed that this same heat treatment may be implemented during periodic preventative maintenance actions prior to crack formation in the joint. This approach is preferable and inexpensive as, unlike a conventional repair, the removal and replacement of parts is not necessary, obsolete parts are not consumed, and damage to boards is eliminated.

This study consists of two parts – firstly failure analysis from the Phase 2 pilot run from the combined sequential environment test to evaluate the expected failure times and modes, followed by analysis of the restorative properties of the thermal treatment that was previously characterized. Nanoindentation was used to evaluate the hardness of two alloys – SAC 305 and Violet – before and after subjecting the alloy to the thermal treatment. Prior to the treatment, the alloy had experienced some amount of simulated service life which is expected to degrade microstructure slightly; the thermal treatment theoretically serves to restore the microstructure and mechanical properties, extending service life. Nanoindentation, while not providing an indication of joint performance as a whole, serves as an excellent comparative technique and will give a preliminary indication of the efficacy of the restoration treatment.

**METHODOLOGY**

**Test Vehicle & Assembly**

The test vehicle design (**Figure 4**) was provided by Honeywell and has been used extensively in our prior work<sup>14,15</sup>. The units for the Phase 2 combined environment pilot run were built at the same time as the units from Phase 1A and Phase 1B at a Curtiss Wright facility in September 2015. The Time Zero assemblies were built in January 2018. Three alloys were selected – SAC 305 (Sn-3.0Ag-0.5Cu), Violet (Sn-2.25Ag-0.5Cu-6.0Bi), and Sn-37Pb.

**Test Conditions**

Three assembly conditions were selected, each representing some instance in the product’s life cycle:

1. Time Zero (T0), representing as-fabricated assemblies. Note that the assemblies in this study were not truly time zero; assembly was conducted approximately seven months before analysis, in January 2018.

2. Room Temperature (RT) Storage, representing ambient storage conditions. The assemblies used for this condition had been assembled in September 2015, indicating approximately 33 months of total aging time.
3. Reliability Tested, representing some duration of heavy product usage. This was conducted via sequential ATC and vibration and is described further below. These assemblies were built at the same time as the RT aged assemblies, indicating that in addition to reliability testing, there was some duration of ambient temperature storage.

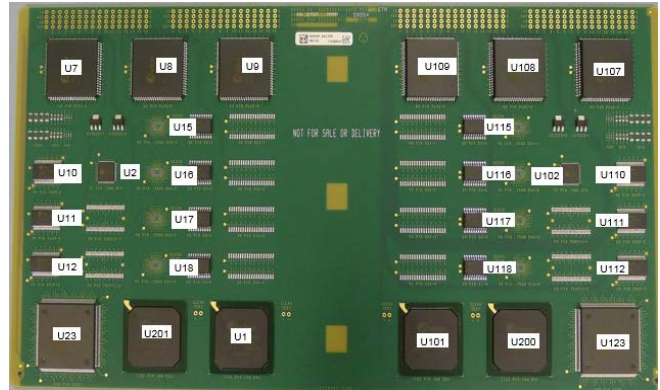


**Figure 4:** Test Vehicle with all part designators labelled.

**Test Matrix**

One board of each metallurgical composition underwent combined ATC and vibration reliability testing along with failure analysis (FA), however due to budget and time constraints, only select parts on SAC 305 and Violet assemblies were tested using the restorative heat treatment; SnPb was excluded. For Violet, both PLCC and BGA parts were examined, and only PLCC parts were examined for SAC. It is important to note that the composition of a Violet PLCC joint is different than a Violet BGA joint, as the BGA parts had SAC 305 balls attached.

**Table 2** indicates the test conditions that were considered in this study. One board of each composition (SAC 305 or Violet) was considered for each assembly condition (1, 2, or 3), for a total of six boards. Each board was cut in half; one half was left as-is (a), while the other was subjected to a heat treatment above the solvus of the Violet alloy (b), for a total of six environmental conditions (1a, 1b, 2a, 2b, 3a, and 3b). Therefore, 18 total sample variations were considered.

**Table 2:** Restoration Treatment Test Matrix

#	Condition	Violet		SAC
		PLCC	BGA	PLCC
1a	Time Zero	U9	U1	U9
1b	Preconditioned	U109	U101	U109
2a	Reliability Tested	TBD	TBD	TBD
2b	Restored 1	TBD	TBD	TBD
3a	Room Temp. Storage	U9	U1	U9
3b	Restored 2	U109	U101	U109

Consistent parts (U1, U9, U101, U109) were selected for analysis across assembly conditions 1 and 3. The parts selected for assembly condition 2 were based on the failure table from the combined environment test (see Results). Parts were chosen which failed electrically later in the test (closer to 2000 ATC cycles and 2 million vibration cycles) where possible, to acquire the best representation of the ‘as-failed’ condition.

### Accelerated Reliability Testing

Sequential ATC and vibration was used to simulate extensive product life. The test consisted of ~100 ATC cycles from -55°C to +125°C followed by ~90,000 vibration cycles (300με, at 75°C). This sequence was repeated twenty times, until ~2000 ATC cycles and ~2 million vibration cycles had elapsed. As only one unit could undergo vibration at any given time, while all three units could undergo ATC, each unit experienced some idle time either before or after vibration.

Four rosettes and eight linear strain gauges were mounted at locations based on the parts and strains of interest across the board assembly (Figure 5). The location of the thermocouple and the response accelerometer were also defined in the test specification. The resistance monitoring cables are hand soldered to the PTH barrels located along the free edge of the unit and all cables: resistance, strain, thermocouples (TC) and accelerometers are strain relieved with Kapton tape or flexible RTV.

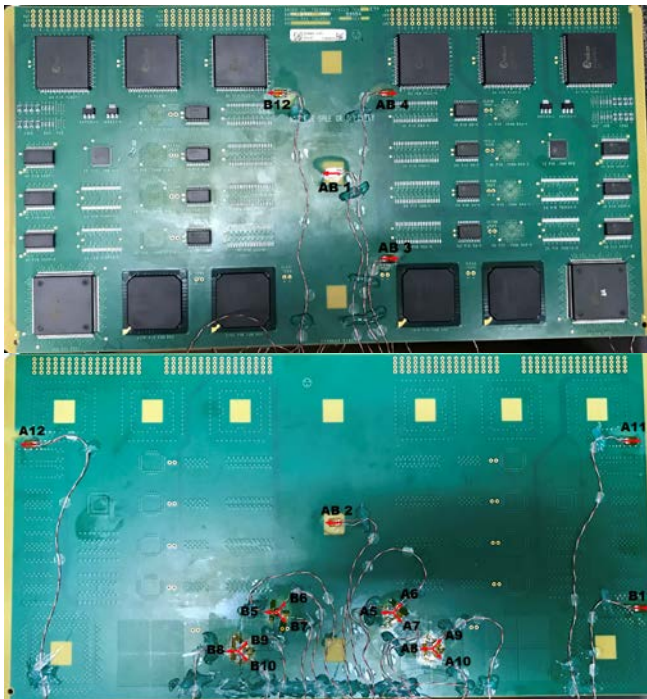


**Figure 5:** Test Vehicle Strain Gauge Layout. Four linear strain gauges were attached on the top side of the assembly (a); the remaining four linear gauges and the four rosettes were attached on the bottom side (b).

ATC was performed to a target of -55°C to 125°C with a ramp rate of 10°C/min and a 15-minute dwell at both extremes, per IPC 9701 specification. Temperature measurements for guiding the profile were measured at the test vehicle component level as opposed to the chamber level. The actual profile resulted in a hot dwell at 130°C for 13 minutes and a cold dwell at -58°C for 12 minutes with a 20 minute ramp in between, totaling 65 minutes per cycle as shown in Figure 6. As mentioned above, all three assemblies were placed into the chamber simultaneously, with air able to circulate freely.

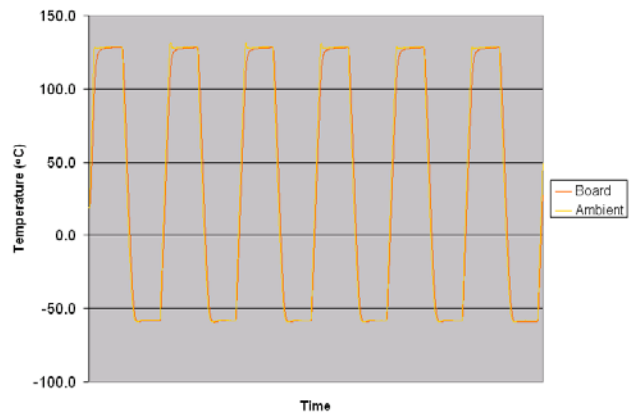


**Figure 6:** ATC Profile

The vibration stress procedure consisted of 3 main steps. The first step was a sine sweep performed at a set G level between 10 and 200 Hz to validate the targeted strain level and associated resonant frequency of the test vehicle. Once targeted strain level is confirmed, the second step is to run a dwell of 20,000 vibration cycles at the defined temperature, at the G level determined from the sweep. A Jaguar software system was utilized to monitor and track to +/- 10% of the targeted resonant frequency of the test vehicle during the run. If the desired constant microstrain level is not being met, steps 1 and 2 are performed again at an updated G level to get to the strain target. The third step in this sequence is a dwell of 70,000 vibration cycles to complete the vibration injection of approximately 90,000 vibration cycles between ATC cycles. Further details on vibration may be found in our earlier work<sup>14,15</sup>.

Analysis Tech STD-256 event detectors were used to monitor the resistance thresholds of 18 components on each board. A failure was recorded when the channel resistance increased to 300Ω or more for at least 200ns. Each recorded failure was checked at room temperature to determine the location of failure, i.e. within the component, a board or trace issue or within the cable connection. Failed components were not removed from the board for failure analysis until the completion of 2000 ATC and 2 million vibration cycles, as this would change the geometry and subsequently the resonance frequency of the board during subsequent vibration cycles.

### Sample Preparation and Failure Analysis

For the failure analysis study, select parts from the three reliability-tested assemblies were removed using a diamond wire saw after testing was completed and mounted in epoxy. Samples were then cross-sectioned to the first row of joints using a series of silicon carbide (SiC) papers, diamond polishing slurries, and a final colloidal silica polish to observe the failure mode. Imaging was conducted using an optical metallographic microscope.

For the restoration study, each SAC and Violet assembly was cut in half along the short axis of the PCB using a band saw; one half was left as-is (Conditions 1a, 2a, 3a) and the other half was heat treated in a furnace. Temperature was carefully monitored using a thermocouple and did not fluctuate more than 1°C from the desired treatment temperature. This process was conducted for the reliability tested assemblies after FA was completed.

The parts listed in **Table 2**, along with additional parts from the reliability tested assemblies, were then cut from the assembly using a diamond wire saw. As sample size is limited by the Electron Backscatter Diffraction (EBSD) sample stub in the Scanning Electron Microscope as well as the stage in the nanoindenter, all parts were carefully cut in quarters; the quadrant closest to the center of the board was cross-sectioned. The remaining quadrants were set aside as backup samples, as needed.

Samples were mounted in epoxy and were cross-sectioned to the first row of joints using the same process as that described above. Mount thickness was limited to a 2cm maximum, once again due to restrictions for EBSD and nanoindentation. Unlike the FA samples, PLCC joints for the restoration study were cross-sectioned from the front rather than the side. While this approach makes it more difficult to interpret the failure mode, it allows for more joints to be sectioned simultaneously, which is important due to the anisotropy of Sn and Sn-based solder alloys, which results in different mechanical properties, depending on grain orientation.

### Electron Microscopy

All electron microscopy was conducted using a SU-3500 Variable-Pressure (VP)-SEM, operated at 15kV and under 50Pa of partial pressure. Using a partial pressure is a necessary alternative to depositing a thin conductive layer such as carbon on the sample surface, as these can interfere with the EBSD analysis. All sectioned joints were quickly surveyed and five were imaged using backscattered electrons (BSE) at 300x and 1000x. Of these five joints, three were selected for further analysis using EBSD.

For EBSD, samples were mounted at a 70° tilt and mapping was performed on an area approximately 85µm x 65µm; using a step size of 0.23µm, each map required approximately 40 minutes of beam time. Further post-processing of the EBSD maps was conducted using HKL

software; orientations shown are given using standard Euler angles.

### Nanoindentation

An Anton-Paar NHT3 instrument was used for nanoindentation measurements. Optical imaging was used to select indent locations – where possible, care was utilized to perform the indents within Sn-rich phases (dendrites or grains) for all samples to minimize error. Six indents were made on each sample, arranged in a 2 x 3 grid, with a spacing of at least 10x the depth or 3x the diameter of a typical indent, per ISO 14577 specification. Four joints per test condition were indented, for a total of 24 indents. A load of 10 mN was held at each site for ten seconds at standard ambient conditions.

## RESULTS AND DISCUSSION

### Failure Data

The combined environment reliability data for each monitored component on the three test vehicles is given in **Table 3**. For each component (cell), two numbers are listed; the first number represents the number of ATC cycles the part had experienced at failure; the second number represents the corresponding number of vibration cycles. The number in bold represents the test during which the failure was first detected.

**Table 3:** Failure Table after Test. Shaded green cells indicate which samples underwent FA. Red text indicates which samples were selected for the restoration study.

Location	Violet	SAC	SnPb
U1 (BGA)	1900 / <b>1800K</b>	855 / <b>740K</b>	570 / <b>450K</b>
U201 (BGA)	NF	NF	<b>1045</b> / 900K
U7 (PLCC)	NF	1900 / <b>1781K</b>	NF
U8 (PLCC)	NF	NF	NF
U9 (PLCC)	NF	<b>952</b> / 900K	NF
U10-U12 SSOP	NF	NF	NF
U15-U18 SO3	NF	NF	NF
U2 (QFN)	855 / <b>720K</b>	855 / <b>720K</b>	760 / <b>630K</b>
U23 (QFP)	NF	NF	NF
U101 (BGA)	760 / <b>660K</b>	<b>952</b> / 900K	<b>331</b> / 270K
U200 (BGA)	NF	NF	800 / 695K
U107 (PLCC)	NF	<b>1969</b> / <b>1800K</b>	NF
U108 (PLCC)	NF	NF	NF
U109 (PLCC)	NF	1520 / <b>1354K</b>	<b>1901</b> / 1800K
U110-U112 SSOP	NF	NF	NF
U115-U118 SO3	NF	NF	NF
U102 (QFN)	475 / <b>360K</b>	760 / <b>630K</b>	1045 / <b>979K</b>
U123 (QFP)	NF	NF	NF

Both BGA parts close to the centerline of the board (U1 and U101) failed for all three alloys; on average Violet > SAC > SnPb. No additional parts failed on Violet. For SAC, four of the six PLCC parts failed; for SnPb, both remaining BGA parts and one of the six PLCC parts failed. Insufficient data was acquired to perform Weibull analysis; this will be completed during the main Phase 2 run, in which more assemblies and parts will undergo combined environmental exposure.

The U2 and U102 parts (QFN) failed earliest in the test, for all three alloys. This was likely because the ground pad was not soldered; in this set of tests (including Phase 1a and 1b) this was done to ensure failures occurred. Previous results<sup>16</sup> indicate that soldering the ground pad would improve reliability, while exhibiting the same failure mechanism.

Based on the data from **Table 3**, appropriate samples were selected for the restoration study for Conditions 2a and 2b (**Table 4**). Where possible, parts were selected which failed later in the test, and were not previously cross-sectioned for FA. The latter requirement is important as a mounted sample cannot be heat treated as the mounting epoxy will melt in the furnace. In addition, the time interval between FA and the restoration study was extensive (roughly eight months) and the sections would have undergone considerable recrystallization and displayed microstructure not representative of as-failed conditions. As a result, none of the four Violet parts selected for the restoration study had failed.

**Table 4:** Updated Restoration Treatment Test Matrix.

#	Condition	Violet		SAC
		PLCC	BGA	PLCC
1a	Time Zero	U9	U1	U9
1b	Preconditioned	U109	U101	U109
2a	Reliability Tested	U9	U201	U7
2b	Restored 1	U109	U200	U107
3a	Room Temp. Storage	U9	U1	U9
3b	Restored 2	U109	U101	U109

**Failure Analysis**

The vast majority of parts (including QFNs) failed in the bulk solder (**Figure 7**), at the component side in the case of the BGA joints.

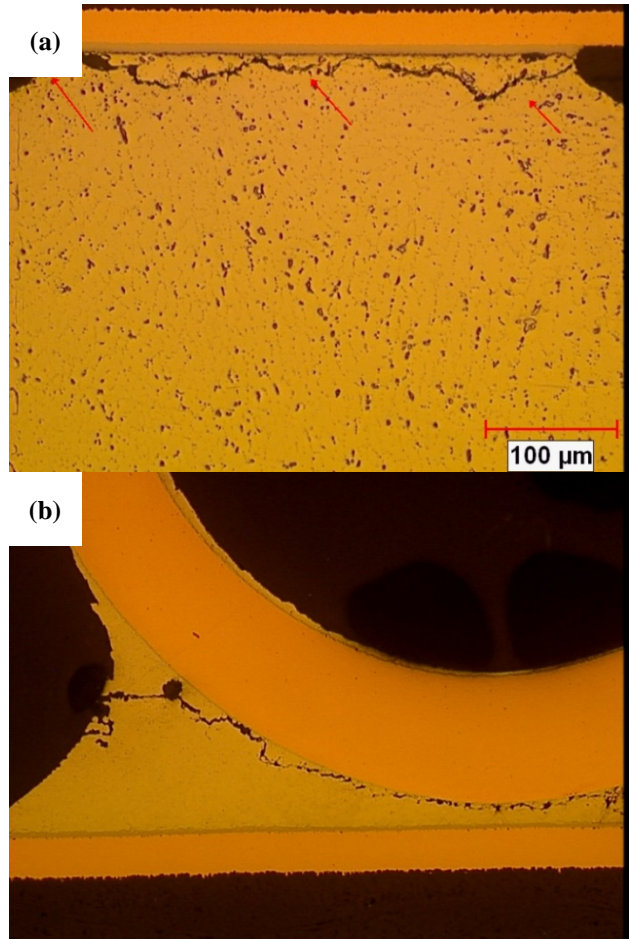


**Figure 7:** Optical micrographs of solder joints after combined environment exposure. Violet BGA (U1), Joint AP17 (a); SAC 305 PLCC (U109), Pin 1 (b).

One notable exception was on the Violet BGA (U101, joints A18 and A21), in which the failure appeared to occur in the component side IMC layer. SEM and EDX were performed on these joints (**Figure 8** and **Table 5**) to verify the failure mode. The samples were coated in a conductive Au layer prior to SEM/EDX analysis, which produced Au peaks in the EDX scans. The EDX results indicate that the separation occurred through the intermetallic layer, indicating that a mixed mode interfacial fracture occurred between the intermetallic and the solder/Ni. The Sn and Ni found on both sides of the separation indicate that both sides are part of the IMC layer. It is possible this failure caused the U101 part to fail earlier than the other BGA on the Violet card (U1) and this is an example of an outlier whose failure mode deviates from the rest of the population.

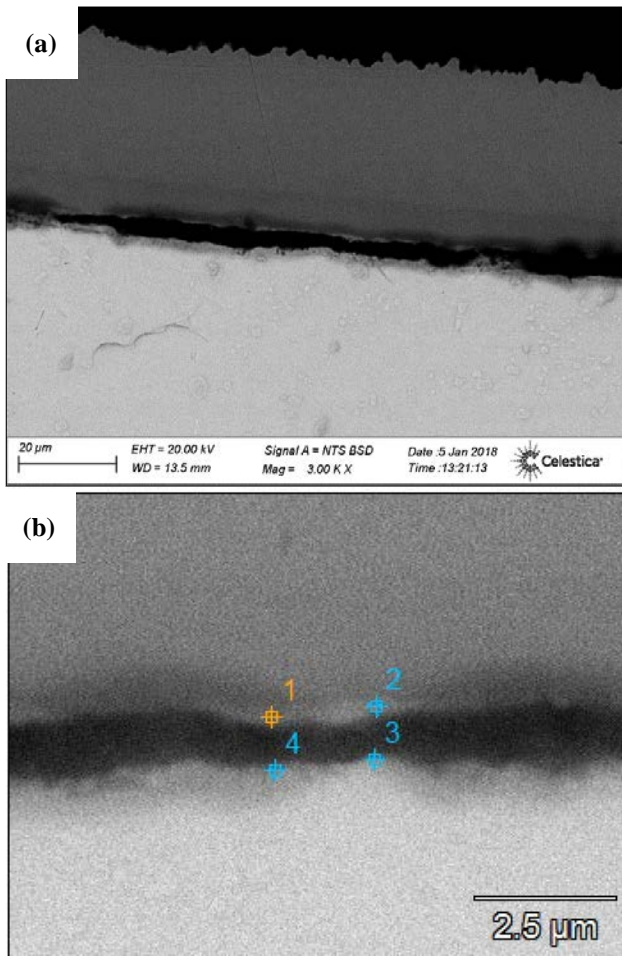


**Figure 8 (starting on previous page):** SEM micrographs of Interfacial Fracture in Violet U101 BGA, Joint A21, low magnification (a); high magnification, showing EDX point scan locations in Table 5 (b).

**Table 5:** EDX Analysis of Violet U101 Ball A21 Interfacial Fracture

#	C	O	Ni	Cu	Sn	Au
1	16.52	12.98	20.19	11.27	35.17	3.87
2	14.13	13.00	25.46	10.80	33.22	3.39
3	14.69	16.07	6.08	8.74	48.80	5.62
4	11.92	13.62	4.61	4.92	61.03	3.91

In addition, EDX was performed on the bulk Ni layer on these joints as well as joints not exhibiting this failure mode, to determine whether high phosphorous content is responsible for the interfacial failure (**Table 6**). It was found that the amount of phosphorous is negligible in both samples, which is expected in typical electrolytic Ni plating.

**Table 6:** EDX Analysis of Ni Layer in Violet BGA Joints

#	C	O	P	Ni	Cu	Sn	Au
U1 AP2	1.95	2.26	0.07	74.37	2.78	15.60	2.97
U101 A18	5.58	2.40	0.06	70.86	3.43	13.85	3.82

## Microstructure Characterization

### SAC 305 PLCC

The SAC 305 PLCC joints display typical dendritic microstructure at T0 (**Figure 9a**), with slight coarsening of the IMCs after preconditioning. This structure is no longer present after reliability testing (**Figure 9b**), with significant coarsening of  $\text{Ag}_3\text{Sn}$  and  $\text{Cu}_6\text{Sn}_5$  IMCs. No difference is observed after the restoration treatment, likely because the duration of the treatment is insignificant compared with the duration of the test.

After extensive RT aging, the dendritic structure persists, with coarser IMCs than at T0, but not as coarse as after reliability testing (**Figure 9c**). Once again the restoration treatment has negligible, if any, effect on the microstructure, because of the same reason discussed above. EBSD (not shown) revealed a coarse grain structure for all conditions, comparable to our earlier work<sup>10</sup>, with Sn recrystallizing at the crack front, indicative of damage accumulation during reliability testing.

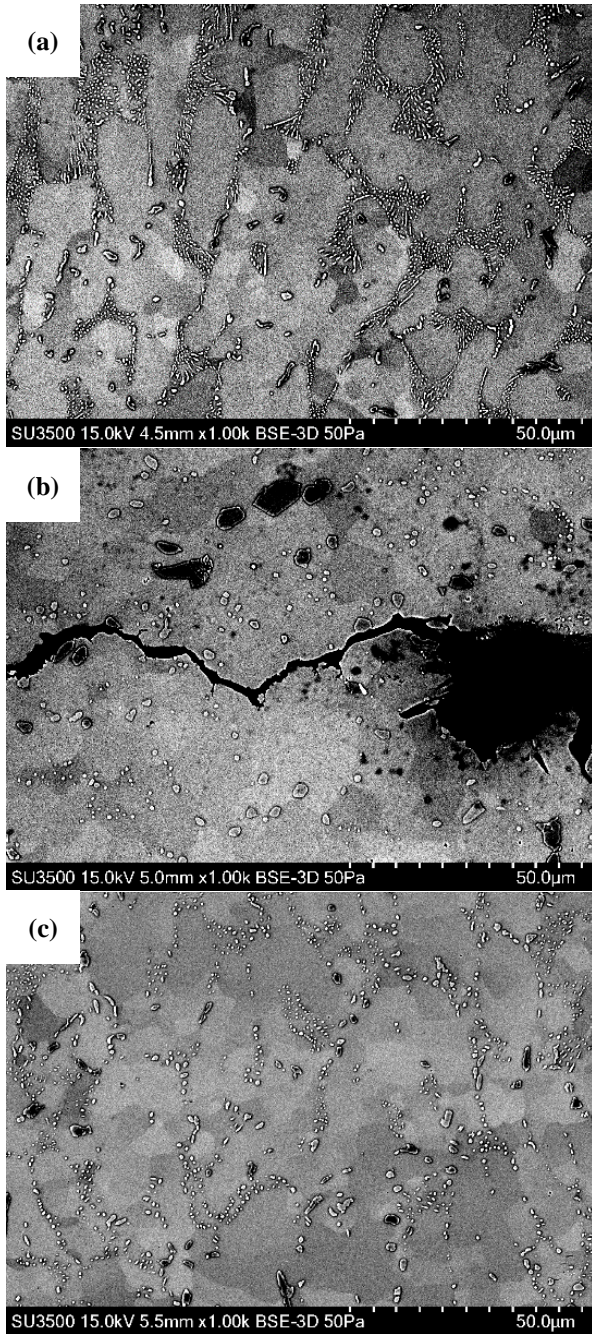


**Figure 9:** Select SEM images from SAC PLCC joints. T0 (a); Reliability tested (b); RT aged (c).

*Violet PLCC*

The Violet PLCC joints also solidified in a dendritic structure, with wider dendrite arm spacing than SAC. Bi precipitates were clustered in the interdendritic spaces (**Figure 10a**), and the grain structure was coarse (**Figure 10b**) with localized recrystallization near Bi precipitates. It is likely, since T0 samples were aged at RT for several months, that some particle coarsening occurred. Some Bi appeared to migrate into the Sn dendrites after preconditioning (**Figure 10c**), and the grain structure is

slightly refined due to more uniform Bi precipitation (**Figure 10d**) than at T0.

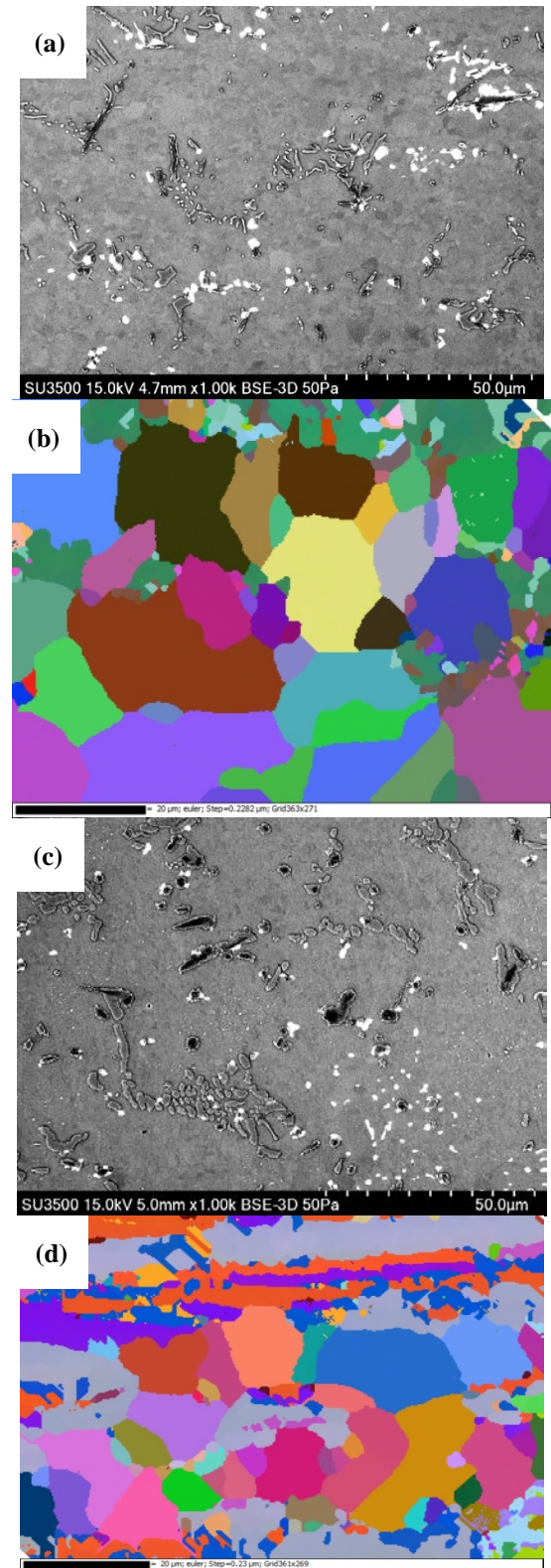
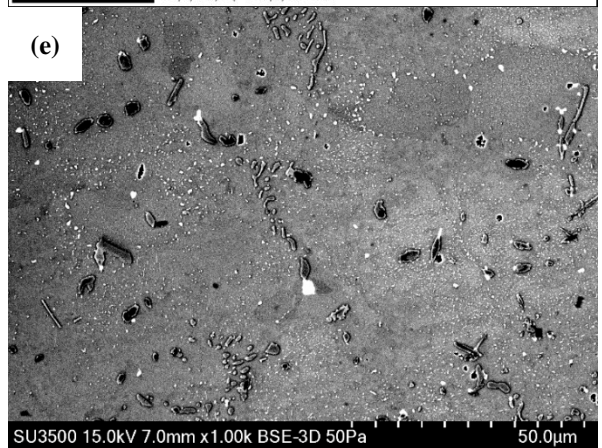
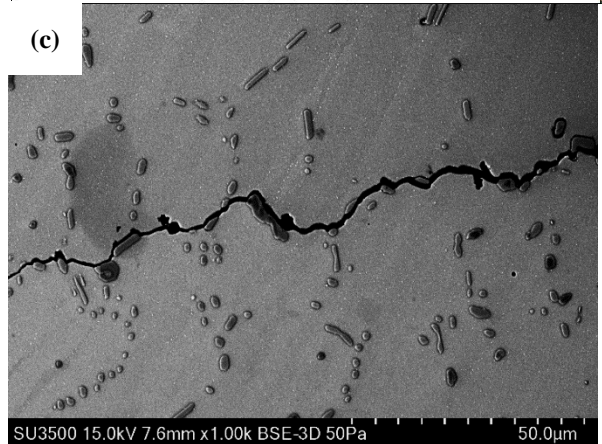
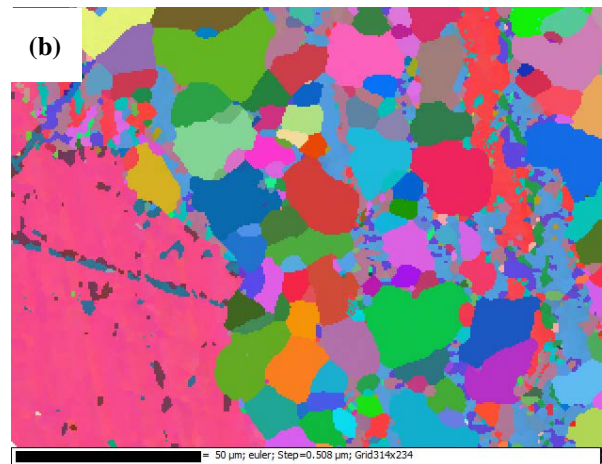
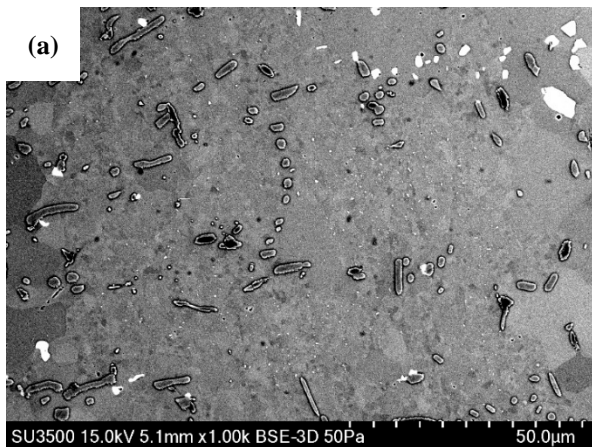


**Figure 10:** Select SEM images and EBSD maps from Violet PLCC joints. T0, SEM (a) and EBSD (b); Preconditioned, SEM (c) and EBSD (d).

After reliability testing, the dendritic structure was lost (**Figure 11a**) and a lower area fraction of Bi precipitates was observed in cross-section, suggesting Bi may have been forced into a supersaturated solid solution. Extensive recrystallization of the Sn matrix occurred (**Figure 11b**). After restoration, submicron Bi precipitates are evenly dispersed throughout the Sn matrix, with no coarsened particles (**Figure 11c**). The Sn grain structure coarsened drastically (**Figure 11d**); a very different result than expected. It was previously observed, in Bi-bearing solder alloys, that recrystallization of the Sn matrix occurs after aging<sup>10</sup>. This is surmised to be caused by density and lattice structure mismatch between Sn and Bi as the latter comes out of solid solution during cooling, stressing the Sn matrix. This is known as Particle Stimulated Nucleation (PSN). Theory of this phenomenon<sup>17</sup> suggests that submicron particles may fail to induce matrix recrystallization – this may explain the coarsened structure observed in these restored samples.

After RT aging, the microstructure of the Violet PLCC joints is comparable to that of the T0 joints. After the restoration treatment, Bi precipitates became more evenly dispersed into the Sn matrix (**Figure 11e**) and are a little coarser than those present in the joints restored after reliability testing. This is accompanied by significant recrystallization of the Sn matrix, producing a fine grain structure (**Figure 11f**).

The restoration treatment produced very different microstructures between the reliability tested and RT aged joints. It is possible that during reliability testing, Bi undergoes more dissolution and diffusion in the Sn matrix at the higher dwell temperature and becomes more distributed than after isothermal aging at ambient temperature. After restoration, the Bi precipitates become finer and more uniformly distributed in the reliability tested samples compared with the RT aged samples. The particle size in the latter is therefore sufficiently large to induce PSN of the surrounding Sn matrix.



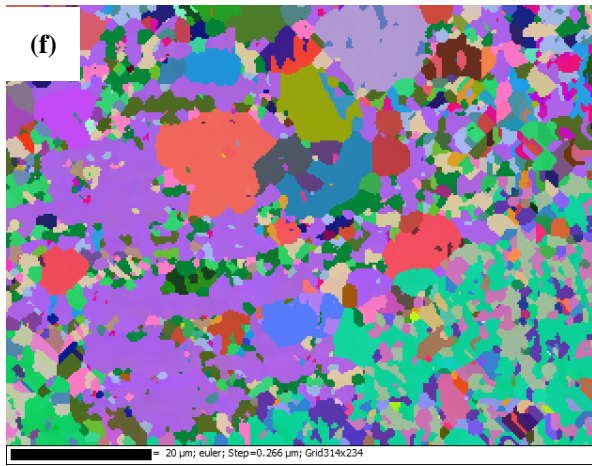


**Figure 11:** Select SEM images and EBSD maps from Violet PLCC joints that had experienced simulated service life. Reliability tested, SEM (a) and EBSD (b); Restored after reliability testing, SEM (c) and EBSD (d); Restored after RT aging, SEM (e) and EBSD (f).

#### Violet BGA

The microstructure and grain structure of the Violet BGA joints closely resembled that of the SAC PLCC joints, with a dendritic structure and very coarse grains (**Figure 12a**). This is likely the result of the BGA ball being composed of SAC 305. Very few Bi precipitates were observed, which is to be expected given the mixed metallurgy of the joint. No observable changes occurred after preconditioning. After reliability testing, the dendritic structure was lost, IMCs underwent coarsening, and some recrystallization was observed, likely caused by damage accumulation during testing (**Figure 12b**). The microstructure after RT aging was very similar to that at T0. No observable changes were observed in either reliability tested or RT aged samples after restoration treatments. Overall, less coarsening of the IMCs occurred than in the SAC PLCCs; this suggests that Bi in solid solution may provide a stabilization effect to the alloy microstructure over time.

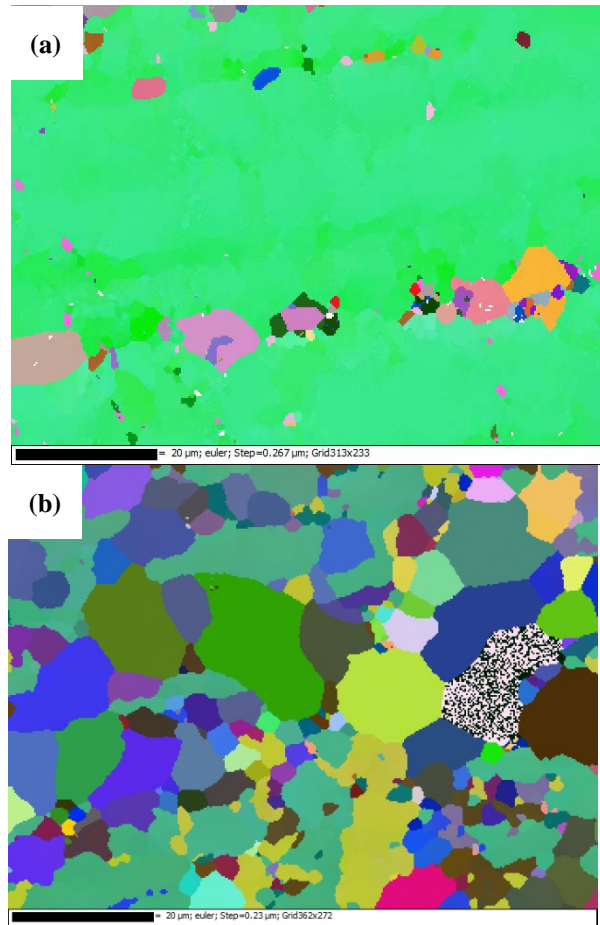


**Figure 12:** Select EBSD maps from Violet BGA joints. T0 (a) and reliability tested (b).

#### Nanoindentation

Nanoindentation hardness results are displayed in **Figure 13** (SAC 305 PLCC), **Figure 14** (Violet PLCC), and **Figure 15** (Violet BGA). In each plot, the data is grouped into the three assembly conditions with the corresponding heat treatment with standard error. Indentation depth measurements, arranged by sample type, are shown in **Table 7**.

**Table 7:** Indentation Depth, by Sample Type (in μm)

Sample Type	Average	Std Deviation
SAC PLCC	1.50	0.08
Violet PLCC	0.95	0.07
Violet BGA	1.20	0.09

For the SAC 305 PLCC joints (**Figure 13**), all environmental conditions yield comparable hardness values with low standard error; this was observed in the microstructure. For SAC 305, hardness typically decreases after aging, however only a slight decrease was observed after preconditioning. This is probably because the T0 joints had been aged at RT for seven months and further aging above solvus did not degrade microstructure significantly further. The same logic can be applied to RT samples compared to the corresponding restored samples. The

hardness of T0 and RT joints were nearly identical - it is possible that seven months of aging is sufficient to minimize the hardness of the alloy and level off, as seen in previous aging studies<sup>2</sup>. As observed above, the coarsening of microstructure was comparable between these two conditions. The hardness of the reliability tested joints was noticeably lower than T0 joints; this is indicative of the damage incurred during testing. Finally, the hardness of the reliability tested joints increased slightly after restoration – this is not expected for SAC and is likely the result of variations in hardness between individual joints, each with different Sn grain orientation.

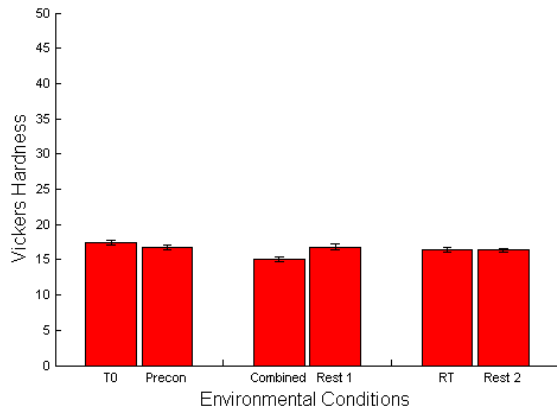


**Figure 13:** Hardness of SAC 305 PLCC joints after environmental exposure and heat treatment.

The Violet PLCC joints (**Figure 14**) demonstrated higher hardness values than their SAC 305 counterparts, likely caused by Bi present in solid solution and as second phase precipitates. The standard error is higher; this may be because there are more second phase particles in the microstructure, resulting in a higher likelihood for the indenter head to contact IMCs and/or Bi precipitates.

All three assembly conditions (T0, reliability tested, and RT aged) show comparable hardness; each had experienced some long-term storage / simulated usage and the degree of microstructure evolution was comparable. The reliability tested samples, however, contained a much sparser distribution of Bi precipitates and it is possible the Sn matrix may be supersaturated with Bi. Preconditioning did not change hardness after T0 statistically; this agrees with results from our prior studies<sup>2</sup> and with the microstructures shown in **Figure 11**.

The hardness of joints that had undergone reliability testing increased appreciably after restoration treatment, indicating the treatment ‘healed’ the microstructure. As observed in **Figure 11c**, Bi precipitates are very fine and evenly dispersed in the Sn matrix, which likely contributes to this improvement in hardness. A similar, but smaller increase in hardness is observed in joints that had experienced long-term isothermal storage – as shown in **Figure 11e**, precipitates are slightly coarser and less dispersed than those

restored after reliability testing. These improvements are likely caused by dissolution of coarse Bi precipitates; these are less effective at strengthening the alloy.

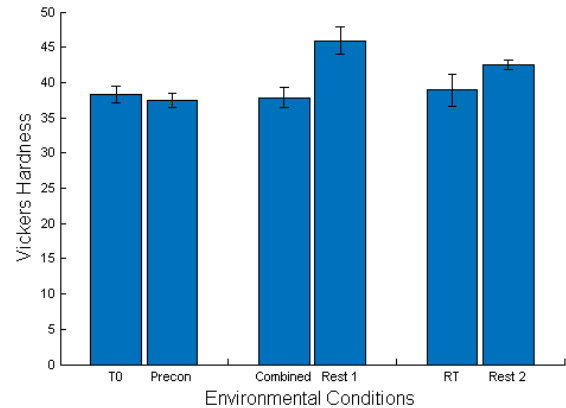


**Figure 14:** Hardness of Violet PLCC joints after environmental exposure and heat treatment.

The Violet BGA joints (**Figure 15**) demonstrated hardness values and standard error intermediate to those of the SAC PLCC and Violet PLCC joints, due to the mixed metallurgy. The three assembly conditions again show comparable hardness, likely due to the same reasons explained above. Similar to the SAC PLCC joints, Violet BGA joints that had been reliability tested show slightly lower hardness than T0 and RT aged joints – this is correlated with slight coarsening of IMCs. The difference is less than that for SAC PLCC, indicating that Bi may mitigate damage accumulation and IMC coarsening. All heat treatment conditions show no statistical difference in hardness from their original assembly conditions, which again can be explained by comparable microstructures. As these joints are mixed metallurgy, few to no Bi precipitates are present in these joints and thus little to no Ostwald ripening is expected. This is a different result from the Violet PLCC joints and indicates the heat treatment may be more beneficial if Bi precipitates are present in the microstructure.

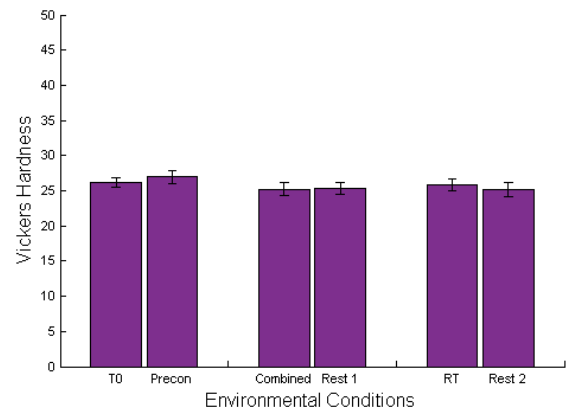


**Figure 15:** Hardness of Violet BGA joints after environmental exposure and heat treatment.

One notable complication from this study is that the parts designated as 'Time Zero' were not truly time zero – they had experienced around seven months of aging at RT between assembly and nanoindentation. It is therefore difficult to ascertain the degree of degradation of the joint after either reliability testing or RT aging, as well as compare the properties of the restored joints to T0 joints.

## SUMMARY & CONCLUSIONS

In this study, we tested the efficacy of our previously patented thermal treatment as a tool for restoring the microstructure and properties of bismuth-containing solder joints after some time in service. This treatment would serve to improve the long term product reliability as part of a normal repair and overhaul (R&O) product plan. The following conclusions can be drawn from this study:

- After sequential combined environment testing, it was observed that Violet outperformed both SAC 305 and SnPb. It is noted that this result was based on a limited cell of one assembly per alloy, and further testing in Phase 2 of our combined environment testing plan will consist of a larger sample size.
- Almost all joints exhibited a consistent failure mode, with crack propagation through the bulk solder. One exception was observed in the U101 BGA part on the Violet assembly, which failed in the component side interfacial IMC.
- The time zero joints in the restoration study, having been built in January 2018, displayed comparable microstructures and hardness as the room temperature aged samples, which had been aging for over two years, for all three alloy-part configurations under test. This indicates that the initial seven months of storage was enough to produce most of the microstructural evolution in these joints.
- For all alloys, parts, and assembly conditions, hardness degraded after reliability testing; this is accompanied by coarsening of IMCs and Sn recrystallization (due to damage accumulation).
- For the Violet PLCC joints, the restoration treatment produced statistically significant increases in hardness, indicating the microstructure was 'rejuvenated.' Bi precipitated out of solution in a fine, uniform distribution; this is a more mechanically robust microstructure.
- The SAC PLCC and Violet BGA joints underwent no discernable changes to microstructure or hardness after restoration treatment. This is possible evidence that the thermal treatment may be more beneficial for improving the properties of joints with ample Bi content, sufficient to form a second phase precipitate.

It is also noted that the results from this study may not be an adequate representation of the performance of the alloy in a practical product. Nanohardness measurements are taken from very small regions of the sample and are only influenced by features on the micro- to nano-scale, including second phase particles, alloy composition, and

grain boundaries. In addition, the mechanical response may be influenced by unseen subsurface second phase particles. Nanoindentation results are independent of features such as joint geometry, package type, and interfacial IMCs, which often factor into performance in reliability testing and product usage. For these reasons, we stress that while the results from this study (namely the Violet PLCC joints) are promising, further work (discussed below) is required to evaluate the efficacy of the restoration treatment on the performance of the alloy as a solder joint in a more practical configuration.

## ONGOING AND FUTURE WORK

The main Phase 2 run is currently underway, in which a larger cell of assemblies (with the same three alloys) will undergo either straight ATC or sequential ATC and vibration testing, as illustrated in **Table 1**. ATC will be performed at one of two temperature ranges: -55°C to 125°C, or -40°C to 85°C, and vibration will be performed at 75°C. For the latter temperature range, some assemblies will undergo preconditioning. Weibull statistical and metallurgical analysis is planned. After the pilot run, it was decided, to induce more failures to allow for sufficient data for statistical analysis, to increase the target strain to 325 $\mu\epsilon$  from 300 $\mu\epsilon$ .

A new cohort of projects under ReMAP will commence in the coming months; these projects are collectively referred to as 'ReMAP 2.0.' Several of these projects will serve as a continuation of the present focus on the commercialization of Bi-containing solder alloys. One project will focus on further characterization of the metallurgy of these alloys through our academic connections; the other will consist of product pathfinder studies, in which assemblies are subjected to more practical environments as opposed to an accelerated test in the lab. There is also interest in conducting restoration treatments on assemblies mid-testing and compare reliability to assemblies that were not subjected to the treatment. This will allow for a more conclusive indication of the efficacy of the restoration treatment on joint performance.

## ACKNOWLEDGEMENTS

We would like to acknowledge the Refined Manufacturing Acceleration Process (ReMAP) for funding this work. In addition, we would like to thank Eric Nicholson, Derek Aranguren, and Chandra Veer Singh from the Department of Materials Science & Engineering at the University of Toronto for assistance with nanoindentation. We would also like to thank the following individuals at Celestica: Kamran Sodaei and Zohreh Bagheri for failure analysis; and Russell Brush, Sutha Subramaniam, and Alex Simpson for chamber work and vibration testing. For assembly services, we thank Thoba Nguyen from Curtiss-Wright.

## REFERENCES

- 1 P. Snugovsky et al., *Reliability Screening of Lower Melting Point Pb-Free Alloys Containing Bi*, APEX Expo 2014, Las Vegas, NV, March 25-27, 2014

- 2 A. Delhaise et al., *The Effects of Bi and Aging on the Microstructure and Mechanical Properties of Sn-rich Alloys*, J. of Surface Mount Technology, 30, 2 (2017), pp. 21-27
- 3 David Witkin, *Mechanical Properties of Bi-containing Pb-Free Solders*, APEX Expo 2013, San Diego, CA, February 16-21, 2013
- 4 H. Ma, J. Suhling, et al., *The Influence of Elevated Temperature Aging on Reliability of Lead Free Solder Joints*, 2007 Electronic Components and Technology Conference, John Ascuaga's Nugget Sparks, NV, USA, May 29-Jun 1, 2007
- 5 M. Hasnine, M. Mustafa, J.C. Suhling et al., *Characterization of Aging Effects in Lead Free Solder Joints Using Nanoindentation*, 2013 Electronic Components and Technology Conference, Las Vegas, NV, USA, May 29-31, 2013
- 6 H. Ma, J. Suhling et al., *Reliability of the Aging Lead-free Solder Joint*, 2006 Electronic Components and Technology Conference, San Diego, CA, May 30-June 2, 2006
- 7 P. Vianco, et al., *Properties of Ternary Sn-Ag-Bi Solder Alloys: Part 1- Thermal Properties and Microstructural Analysis*, J. Electronic Materials, 28, 10 (1999), pp. 1127-1137
- 8 P. Vianco, et al., *Properties of Ternary Sn-Ag-Bi Solder Alloys: Part 2- Wettability and Mechanical Properties Analysis*, J. Electronic Materials, 28, 10 (1999), pp. 1138-1143
- 9 A. Delhaise et al., *Microstructure and Hardness of Bi-containing Solder Alloys after Solidification and Aging*, J. Surface Mount Technology, 27, 3 (2014), pp. 22-27
- 10 A. Delhaise et al., *Thermal Preconditioning, Microstructure Restoration, and Property Improvement in Bi-Containing Solder Alloys*, J. Surface Mount Technology, 31, 1 (2018), pp. 33-42
- 11 A. Delhaise et al., *Effect of Thermal Treatment on the Microstructure, Properties, and Reliability of Lead-Free Bi-Containing Solder Alloys*, 2017 SMTA International Conference, Rosemont, IL, September 17-21, 2017
- 12 A. Mayyas et al., *Recrystallization of Lead-free Solder Joints-Confounding the Interpretation of Accelerated Thermal Cycling Results*, ASME 2009 International Mechanical Engineering Congress & Exposition, Lake Buena Vista, FL, November 13-19, 2009
- 13 A. Perkins, S.K. Sitaraman, *A Study into the Sequencing of Thermal Cycling and Vibration Tests*, IEEE 2008 Electronics Components & Technology Conference, Location, State, Date, 2008
- 14 J. McMahan et al., *Protocol Development for Testing Solder Reliability in Combined Environments*, 2016 SMTA International Conference, Rosemont, IL, September 25-29, 2016
- 15 I. Tan et al., *Accelerated Life Testing Solder Reliability in Combined Environments: Iso Temperatures With Harmonic Vibration*, J. Surface Mount Technology, 31, 1 (2018), pp. 13-24
- 16 D. Hillman, *An Examination of Bottom Terminated Component (BTC) Technologies: Assembly Qualification, Characterization and State-of-Readiness Assessment*, Rockwell Collins Internal Working Paper, WP13-2028, 2013
- 17 F. Humphreys, M. Hatherly, *Recrystallization and Related Annealing Phenomena*, Oxford, UK: Elsevier, 2009